Journal of Biomechanics 113 (2020) 110105

Contents lists available at ScienceDirect

Journal of Biomechanics

journal homepage: www.elsevier.com/locate/jbiomech
www.JBiomech.com

Low-cycle full-field residual strains in cortical bone and their influence on tissue fracture evaluated via in situ stepwise and continuous X-ray computed tomography

Marta Peña Fernández [a,b,*], Alexander P. Kao [b], Frank Witte [c], Hari Arora [d], Gianluca Tozzi [b]

[a] Department of Engineering Mechanics, School of Engineering Sciences, KTH Royal Institute of Technology, Stockholm, Sweden
[b] Zeiss Global Centre, School of Mechanical and Design Engineering, University of Portsmouth, Portsmouth, UK
[c] Biotrics Bioimplants AG, Berlin, Germany
[d] College of Engineering, Swansea University, Swansea, UK

ARTICLE INFO

Article history:
Accepted 20 October 2020

Keywords:
Cortical bone
In situ mechanics
Cyclic loading
X-ray computed tomography
Digital volume correlation
Residual strains

ABSTRACT

As a composite material, the mechanical properties of bone are highly dependent on its hierarchical organisation, thus, macroscopic mechanical properties are dictated by local phenomena, such as microdamage resulting from repetitive cyclic loading of daily activities. Such microdamage is associated with plastic deformation and appears as a gradual accumulation of residual strains. The aim of this study is to investigate local residual strains in cortical bone tissue following compressive cyclic loading, using in situ X-ray computed tomography (XCT) and digital volume correlation (DVC) to provide a deeper insight on the three-dimensional (3D) relationship between residual strain accumulation, cortical bone microstructure and failure patterns. Through a progressive in situ XCT loading–unloading scheme, localisation of local residual strains was observed in highly compressed regions. In addition, a multi-scale in situ XCT cyclic test highlighted the differences on residual strain distribution at the microscale and tissue level, where high strains were observed in regions with the thinnest vascular canals and predicted the failure location following overloading. Finally, through a continuous in situ XCT compression test of cycled specimens, the full-field strain evolution and failure pattern indicated the reduced ability of bone to plastically deform after damage accumulation due to high number of cyclic loads. Altogether, the novel experimental methods employed in this study, combining high-resolution in situ XCT mechanics and DVC, showed a great potential to investigate 3D full-field residual strain development under repetitive loading and its complex interaction with bone microstructure, microdamage and fracture.

1. Introduction

Cortical bone is a complex composite material whose structure is hierarchically organized from the nano- to the macroscale to withstand physiological loads and resist fracture (Wolfram and Schwiedrzik, 2016). Yet, the mechanical competence of bone is often impaired by the accumulation of microdamage due to isolated overloading events (Gauthier et al., 2019; Morgan et al., 2005) or after suffering fatigue from a large number of loading cycles (Burr et al., 1997; Diab et al., 2006; Schaffler et al., 1995; Zioupos and Currey, 1998). Microdamage in cortical bone tissue is manifested in the form of microcracks or diffuse damage (O'Brien et al., 2007). Microcracks, in particular, are thought to play an important role in bone fracture behavior as well as in bone remodelling, mechanotransduction and the bone toughening mechanism (Voide et al., 2009). The formation of microcracks is dependent on the loading mode, (Mirzaali et al., 2015; Reilly and Currey, 1999) and they are also influenced by the morphological complexity and porosity of cortical bone (Loundagin et al., 2020; Turnbull et al., 2014). Under cyclic loading, microcracks can grow and cause fractures in bone, clinically known as stress fracture (Zioupos et al., 1996), thus there is considerable interest in understanding the failure mechanism of cortical bone following cyclic loading.

The mechanics of cortical bone subjected to cyclic loading has been previously investigated with a focus on the fatigue life and microcrack propagation (Fletcher et al., 2014; Kim et al., 2007; Nalla et al., 2005; Zioupos et al., 2008; Zioupos et al., 2001).

* Corresponding author: Department of Engineering Mechanics, School of Engineering Sciences, KTH Royal Institute of Technology Osquars Backe 18, 100 44, Stockholm, Sweden.
E-mail address: martapf@kth.se (M. Peña Fernández).

https://doi.org/10.1016/j.jbiomech.2020.110105
0021-9290/

Traditionally, the degradation in the mechanical properties due to repetitive loads has been derived from micromechanical tests (i.e. cyclic tensile/compressive loading) using damage indicators such as modulus reduction in relation to the cycle number and residual strains upon unloading (Bajaj et al., 2014; Fleck and Eifler, 2007; Winwood et al., 2006a, 2006b). Residual strains are generally assessed as the translation along the strain axis at zero stress from traditional stress–strain curves, thus being a measurement of the plastic deformation of the material (Winwood et al., 2006a, 2006b). The influence of residual strain in the fatigue life and strength of cortical bone has been characterized in several studies (Fleck and Eifler, 2007; Morgan et al., 2005; Winwood et al., 2006a, 2006b); however, how the microarchitecture affects the fatigue life of bone and, in particular, the residual strain accumulation is still lacking, mainly due to the difficulty of relating the macroscopic mechanical behavior to the cortical bone microstructure. Since the structure-mechanics relationship is a key factor in bone damage, a three-dimensional (3D) characterization of the residual strains due to cyclic loading remains essential.

To date, the only experimental technique that allows for 3D full-field strain is digital volume correlation (DVC), which in combination with X-ray computed tomography (XCT) has been extensively used in bone mechanics to investigate the deformation mechanism under different loading conditions (Christen et al., 2012; Peña Fernández et al., 2020, 2019). Particularly, Christen et al. (2012) investigated the role of cortical bone microstructure in the initiation and propagation of microcracks in notched cortical bone specimens under compression by measuring the local strains in the tissue, revealing the complex interaction between microcrack propagation and bone microarchitecture. However, the measured strains resulted from time-lapsed compression testing, while the effect of cyclic loading and residual strains upon unloading were not the object of that study. The potential of DVC in evaluating residuals strains under cyclic compression has been previously explored by Tozzi et al. (2014) in bone-biomaterial composites. The progressive damage accumulation under cyclic loading at the bone-biomaterial interface was shown, as evidenced by the initiation of cracks associated with high residual strains. Nevertheless, the intricacy of such biphasic structure together with the limited resolution of the XCT images (i.e. 20 μm) achieved, could not allow the characterization of local residual strain within bone tissue as well as its spatial correlation with bone microstructure. Therefore, by using high-resolution XCT in combination with cyclic mechanical testing and DVC an in depth understanding of the local residual strain in cortical bone tissue will be enabled.

In this work, a series of experiments were carried out in order to assess the ability of DVC based on high-resolution XCT images to evaluate 3D full-field residual strains in cortical bone tissue subjected to low-cycle compressive loading. In particular, this study aims at investigating the residual strain accumulation in relation to the applied level of compression and number of cycles as well as the spatial correlation of local residual strains, intracortical porosity and failure patterns following a compressive overload.

2. Materials and methods

2.1. Specimen preparation

Cortical bone specimens were obtained from the diaphysis of a fresh bovine femur. A 20 mm-thick section was cut from the middle of the femur and a diamond-coated coring tool was used to extract 4 mm diameter cylindrical plugs. The ends of the specimens were then trimmed with a bandsaw to achieve a 10 mm length. All cutting occurred under constant water irrigation and all specimens were wrapped in gauze, soaked in phosphate buffered saline (PBS) and stored at −20 °C until testing. Prior to the experiment the ends of the specimen were cleaned, dried and embedded into brass endcaps using a custom jig to minimize testing uncertainties and achieving a nominal final length of 8 mm (2:1 aspect ratio).

2.2. In situ XCT mechanical testing

The specimens were divided in three groups and underwent three different in situ XCT mechanical tests, as described in Table 1 and Fig. 1.

2.2.1. Progressive compression test

Cortical bone specimens (n = 3) were placed within an environmental chamber filled with PBS in a micromechanical device (CT500, Deben Ltd, UK) that was positioned in the chamber of a high-resolution X-ray microscope (Versa 510, Zeiss, USA) (Fig. 1-I). First, a preload of ~50 N was applied to ensure end contact prior to testing followed by in situ uniaxial compression test at incremental strains of 0.5%, 1% and 2% using a progressive load-unload-reload scheme (Fig. 1-I, right) (Nyman et al., 2009a, 2009b). In each cycle, the specimen was first loaded under displacement control to the target deformation level at a rate of 1 mm/min; then held steady for image acquisition. Thereafter, the specimen was unloaded to zero-strain state (preload configuration) and held there for image acquisition, and then reloaded again to the next strain level. At each loaded-unloaded state XCT images were acquired (80 keV, 7 W, 3.5 μm voxel size, 2.5 s exposure time, 1800 projections), after two repeated scans in the preload configuration for DVC zero-strain error analysis (Dall'Ara et al., 2017). In total, eight tomographic datasets were acquired for each specimen.

2.2.2. Multi-scale cyclic compression test

In situ XCT uniaxial cyclic compression testing of cortical bone specimens (n = 3) was performed using a loading stage (CT5000, Deben Ltd, UK) placed in the X-ray microscope (Versa 510, Zeiss, USA) (Fig. 1-II). Specimens were mounted within a custom-made chamber and immersed in PBS throughout the test. Prior to cyclic testing, XCT images of the intact specimens were acquired at two different resolutions for a multi-scale evaluation. First, an overall XCT scan (110 keV, 10 W, 5 μm voxel size, 5 s exposure time, 1200 projections) was performed to include the entire specimen diameter within the field of view (FOV, 5 mm × 5 mm); then, a high-resolution XCT scan (80 keV, 7 W, 2 μm voxel size, 12 s exposure time, 1600 projections) of the centre of the specimen (FOV: 2 mm × 2 mm) was acquired. Following acquisition of the first pair of XCT images, each of the specimens was subjected to 5, 30 or 100 cycles of uniaxial compression at a maximum strain of 0.5% and a frequency of 0.2 Hz, after which the XCT imaging procedure was repeated (unloaded state). Finally, specimens were loaded monotonically up to failure and XCT scans acquired after the load was released. In total, three (i.e. intact, cycled and failed) pairs (i.e. 5 μm and 2 μm voxel size) of images were acquired for each sample. Two additional cortical bone specimens were imaged in the same conditions twice consecutively to allow for DVC zero-strain error analysis (Dall'Ara et al., 2017).

2.2.3. Continuous compression test after cyclic loading

In situ SR-XCT continuous compression testing (n = 3) was performed at the Diamond-Manchester Imaging Branchline I13-2 of Diamond Light Source (UK) (Fig. 1-III). A filtered, partially coherent, polychromatic 'pink' beam (5–35 keV) of near-parallel geometry with an undulator gap of 5 mm was used. Projections were recorded by a sCMOS pco.edge 5.5 (PCO AG, Germany) detector, coupled to a 500 μm-thick $CdWO_4$ scintillator and a visual light microscope with a 2× objective lens. Pixel binning (4×) was used

Table 1
Description and aims of the in situ XCT mechanical tests performed in this study. n: number of cortical bone specimens. DLS: Diamond Light Source.

Experiment	XCT system	Loading stage	n	Aim
Progressive compression test	Zeiss Versa 510	Deben CT500	3	To explore the capability of DVC to assess differences between volumetric and residual strains.
Multi-scale cyclic compression test	Zeiss Versa 510	Deben CT5000	3	To examine the spatial correlation between localized strains, intracortical porosity and failure patterns after overloading in a multiscale manner.
Continuous compression test	I13-2 DLS	Deben CT5000	3	To investigate differences in volumetric strain progression and failure mechanism in relation to the number of applied cyclic loads.

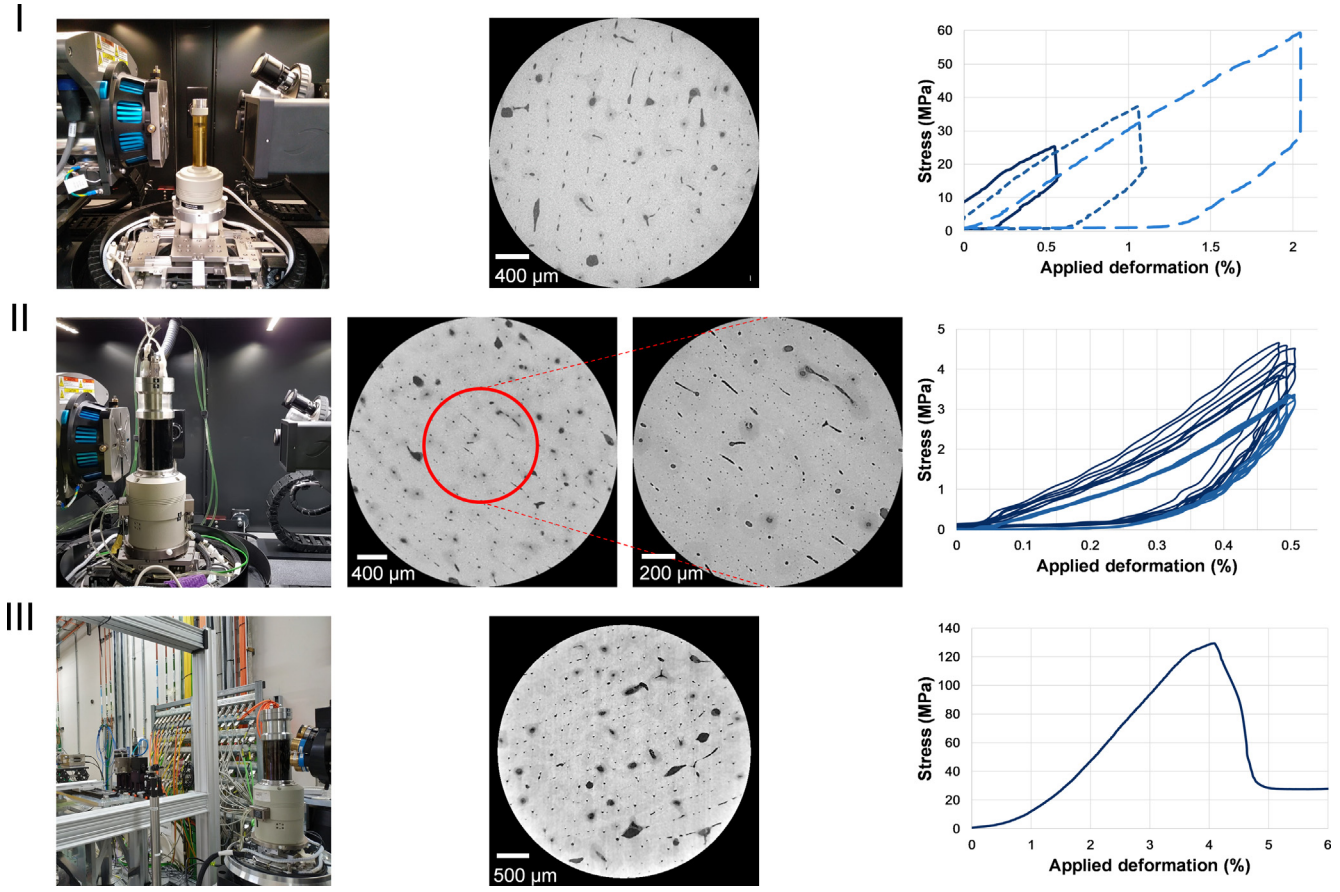

Fig. 1. Summary of in situ XCT experiments performed for this study. I) in situ XCT progressive compression test; II) multi-scale in situ XCT cyclic compression test; III) in situ SR-XCT continuous compression test. The different experimental setups (left) are shown next to a representative XCT cross-section (middle) of the cortical bone specimens and a typical stress-strain curve (right) for each experiment.

to achieve better signal and faster framerates, resulting in an effective voxel size of 6.5 µm and a FOV of 4.2 × 3.5 mm. 1441 projection images were collected over 180° of continuous rotation with a exposure time of 15 ms (plus 2 ms read-out), resulting in an estimated radiation dose of ~0.53 kGy/tomogram (Peña Fernández et al., 2018). Specimens were placed within the PBS-filled environmental chamber of the loading device (CT5kN, Deben Ltd, UK) and subjected to 5, 30 or 100 cycles of uniaxial compression (0.5% maximum strain, 0.2 Hz). Following the cyclic loading scheme, a preload (50 N) was applied to ensure end-contact and continuous loading was performed at a constant crosshead speed of 0.01 mm/min up to failure, with SR-XCT images acquired simultaneously. For all specimens, two repeated scans (preload state) prior to loading were acquired for DVC zero-strain error analysis (Dall'Ara et al., 2017). In total, 18, 16 and 13 tomograms were acquired for the specimen cycled 5, 30 and 100 times, respectively; thus, the total radiation dose remained below 15 kGy, minimizing the possibility of radiation-induced damage (Barth et al., 2010; Marta Peña Fernández et al., 2018; Barth et al., 2010; Peña Fernández et al., 2018).

2.3. Image postprocessing

XCT images acquired in the lab-system were reconstructed using the manufacture's software (TXM Reconstructor, Zeiss, USA). Following image reconstruction, the XCT datasets were rigidly aligned using as reference the first acquired tomogram and denoised using a non-local means filter (Avizo 9.4, ThermoFisher, US). Intracortical porosity was segmented using Otsu's thresholding and the vascular canal network was separated from the osteocyte lacunae by removing the unconnected objects with a volume below 500 μm^3 (Cardoso et al., 2013). The morphometry of the canal network was determined by the total canal volume (Ca.V), canal volume density (Ca.V/Ct.TV) and mean canal diameter

(Ca.D) using BoneJ (Doube et al., 2010) plugin in FIJI (Schindelin et al., 2012).

SR-XCT images were flat-field and dark-field corrected prior to image reconstruction using Savu (Atwood et al., 2015), which incorporated ring artefact suppression. Dedicated Matlab (v2018a, MathWorks, USA) scripts were developed to rigidly aligned the deformed datasets to the reference (unloaded) and to denoise them using an anisotropic diffusion filter.

2.4. Digital volume correlation

DVC (DaVis v10.05, LaVision, Germany) analysis was performed to evaluate the 3D full-field strains in cortical bone specimens subjected to the different mechanical tests. The DaVis software is based on a local approach of deformable registration and further details on the operating principles of the algorithm are detailed elsewhere (Peña Fernández et al., 2018). The acquired zero-strain repeated scans were used to evaluate strain uncertainties (i.e. mean absolute strain (MAER) and standard deviation of the error, SDER (Palanca et al., 2016)) with sub-volumes ranging from 8 to 80 voxels. The final DVC-schemes used for each in situ XCT test and the corresponding strain errors are summarized in Table 2.

Volumetric strain (Eq. (1)) was computed for the evaluation of the strain distribution in specimens under compressive load (Fig. 1-I, III), whereas von Mises Equivalent strain (Eq. (2)) was used to assess the residual strain distribution after unloading (Fig. 1-I) or cyclic testing (Fig. 1-II).

$$\varepsilon_{vol} = \varepsilon_1 + \varepsilon_2 + \varepsilon_3 \tag{1}$$

With ε_1, ε_2 and ε_3 being the principal strains.

$$\varepsilon_{eq} = \frac{2}{3}\sqrt{\frac{3\left(e_{xx}^2 + e_{yy}^2 + e_{zz}^2\right)}{2} + \frac{3\left(\gamma_{xy}^2 + \gamma_{xz}^2 + \gamma_{yz}^2\right)}{4}}$$

$$e_{xx} = \frac{2}{3}\varepsilon_{xx} - \frac{1}{3}\varepsilon_{yy} - \frac{1}{3}\varepsilon_{zz}$$

$$e_{yy} = \frac{2}{3}\varepsilon_{yy} - \frac{1}{3} - \varepsilon_{xx} - \frac{1}{3}\varepsilon_{zz}$$

$$e_{zz} = \frac{2}{3}\varepsilon_{zz} - \frac{1}{3} - \varepsilon_{xx} - \frac{1}{3}\varepsilon_{yy}$$

$$\gamma_{ij} = 2\varepsilon_{ij} \tag{2}$$

3. Results

3.1. In situ XCT progressive compression

Cortical bone specimens subjected to progressive compression test presented small differences in their morphology (i.e. Ca.V/Ct.TV = 2.6 ± 0.4% and Ca.Dm = 55.8 ± 8.5 μm) and apparent elastic modulus (E_{app} = 2.82 ± 0.11 GPa). The highest modulus correlated to the lowest canal volume and the thinnest canals. The internal strain distribution (i.e. ε_{vol} and ε_{eq}) showed a similar pattern for the three specimens. A progressive strain accumulation for both loaded (ε_{vol}) and unloaded (ε_{eq}) states was observed at increasing applied strain amplitudes, with the absolute value of ε_{vol} higher than ε_{eq} at all steps (Fig. 2). Maximum local compressive strains ($\varepsilon_{vol} < 0$) were higher than tensile ($\varepsilon_{vol} > 0$) and residual strains (ε_{eq}) (Fig. 2a), with more than 10% of cortical bone volume showing local compressive values below −4000 με at 2% compression for all specimens; whereas tensile strains remained always below 4000 με and less than 2% of bone volume experienced residual strains above 4000 με. All specimens showed a non-uniform strain distribution, with local strains building up during compression (Fig. 2b, c). The spatial co-localization of highly strained regions in loaded and unloaded states is shown in Fig. 3 and it highlights the predominance of negative ε_{vol}. Residual strains after each incremental applied compression accumulated in cortical bone regions that were previously highly compressed.

3.2. In situ multiscale XCT cyclic testing

Increasing the resolution from 5 μm to 2 μm for the multiscale XCT imaging allowed to identify not only the cortical canal network but also the osteocyte lacunae (Fig. 1-II), resulting in improved DVC spatial resolution from 320 μm to 96 μm, which led to different internal strain distributions for the overall scan (Fig. 4a) compared to the zoom-in region (Fig. 4b). The overall residual strains (ε_{eq}) were highly homogeneous for all the specimens and a slight increase of ε_{eq} values after 100 cycles was observed compared to the less cycled specimens (Fig. 4a). A more complex and heterogeneous ε_{eq} distribution was experienced at tissue level (Fig. 4b), with local strains exceeding those measured at a lower resolution and reaching maximum values over 2000 με in some areas. Such local strain concentrations were more important after 100 cycles of compression. Highly strained regions were found around thinnest canals for all the specimens (Fig. 5a, b). The specimens subjected to 5 and 30 cycles showed longitudinal cracks after failure (Fig. S3), which were localised in proximity to the previously identified areas with high residual strains (Fig. 5c). No visible damage was identified within the FOV of the highest resolution image of the most cycled specimen (Fig. 5c) and only small cracks were observed when examining the entire FOV (Fig. S3).

3.3. In situ SR-XCT continuous compression

The evolution of ε_{vol} during continuous compression for the specimens subjected to 5, 30 and 100 cycles is shown in Fig. 6 in terms of average and standard deviation of strain in the analysed volumes. All samples presented an almost linear increasing trend on the average ε_{vol} values prior to failure. Strain heterogeneity increased after yielding and built-up on the onset of crack formation (Supplementary Video 1). Failure occurred earlier for the most cycled specimen at a lower average ε_{vol} (~−1600 με) compared to the specimens cycled 5 or 30 times, which experienced minimum ε_{vol} of ~−4000 με before failure (Fig. 6). The strain distribution was highly homogeneous for the all specimens prior to failure and heterogeneity in the strain field only increased when cracks were

Table 2
Summary of DVC-schemes used for each experiment and the corresponding strain uncertainties (MAER, SDER) for the n number of specimens analysed. MAER and SDER are reported as mean (standard deviation).

Experiment	Voxel size (μm)	DVC scheme (voxel)	n	MAER (με)	SDER (με)
Progressive compression test	3.5	64-56-48-40	3	401 (126)	101 (37)
Multi-scale cyclic compression test	5.0	88-80-72-64	2	207 (11)	82 (8)
	2.0	72-64-56-48	2	220 (33)	122 (16)
Continuous compression test	6.5	72-64-56-48	3	467 (24)	112 (11)

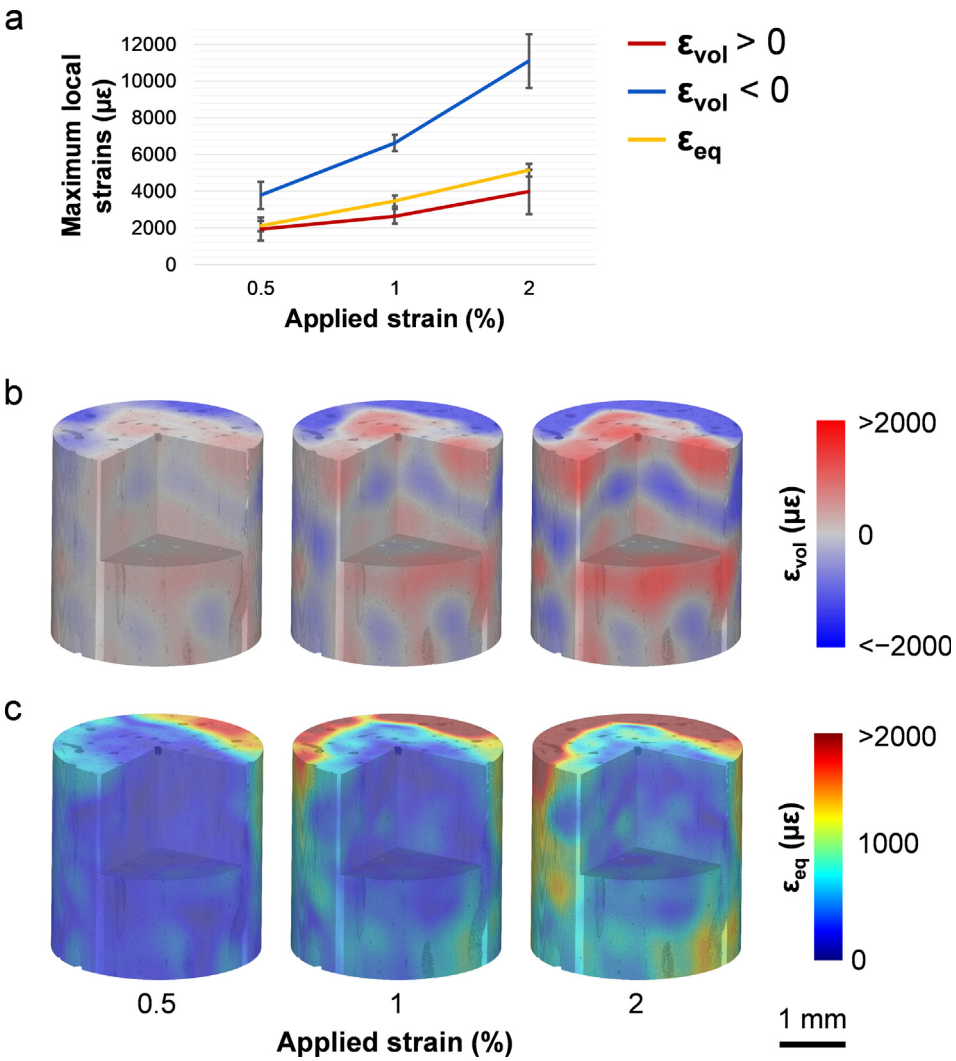

Fig. 2. DVC-computed strains for in situ XCT progressive compression test. (a) The maximum tensile ($\varepsilon_{vol} > 0$), compressive ($\varepsilon_{vol} < 0$) and equivalent von Mises (ε_{eq}) local strains is shown (color-coded) at each incremental compression step, with straight lines joining the mean values and error bars indicating the standard deviation between the three analysed specimens. Full-field (b) volumetric (ε_{vol}) and (c) equivalent von Mises equivalent (ε_{eq}) strain distribution of a representative specimen for the three incremental steps of compression. Strain maps for all specimens may be found in supplementary material Fig. S1, S2.

visible (Fig. 7), with positive ε_{vol} in regions of crack opening and negative ε_{vol} in regions highly compacted. The damage initiation and progression between the specimens was different, with the less cycled specimens displaying a structural collapse due to the presence of a main longitudinal crack running through the entire cortical volume, while cracks in the more cycled specimen did not pierce the volume longitudinally (Supplementary Video).

4. Discussion

The accumulation of microdamage during cyclic loading plays a key role in weakening cortical bone and leading to complete fracture as a result of the degradation in its mechanical properties, which is evidenced by the development of residual strains upon unloading. The main goal of this study was to explore the capability of DVC to assess local residual strains in cortical bone tissue following in situ XCT cyclic loading in order to gain a greater understanding of the 3D relationships between residual strain accumulation, cortical bone microstructure and failure pattern.

The first experiment herein presented aimed at investigating the spatial correlation between volumetric strains in loaded cortical bone specimens and residual strains upon unloading following a progressive loading scheme (Fig. 1-I) similar to that introduced by Wang and Nyman (2007). Maximum ε_{vol} and ε_{eq} local strains in the tissue increased in a nearly linear relationship with the applied deformation (Fig. 2), consistent with the observations of Nyman et al. (2009a, 2009b). DVC-computed ε_{eq} were used as a non-directional measurement of the residual (plastic) local strains (Morgeneyer et al., 2014); this enabled a good representation of the strain localization with respect to bone microstructure and allowed a direct comparison with ε_{vol} in the loaded specimens (Figs. 2 and 3). In this study, the DVC computation successfully showed the coupling of residual strain accumulation and highly compressed regions at low levels of global strains (Fig. 3). Similar findings were observed by Tozzi et al. (2014) in bone-biomaterial composites, where high residual strains after cyclic loading were found in the most strained regions during uniaxial compression. However, the XCT spatial resolution achieved in that study (i.e. 20 μm) did not allow for an in-depth characterization of localized residual strain within the bone tissue.

The multi-scale in situ XCT cyclic test evidenced differences on the residual strain distributions after cyclic loading at different dimensional scales (Fig. 4). Despite the ε_{eq} was found to slightly increase with higher number of cycles at the microscale (Fig. 4a),

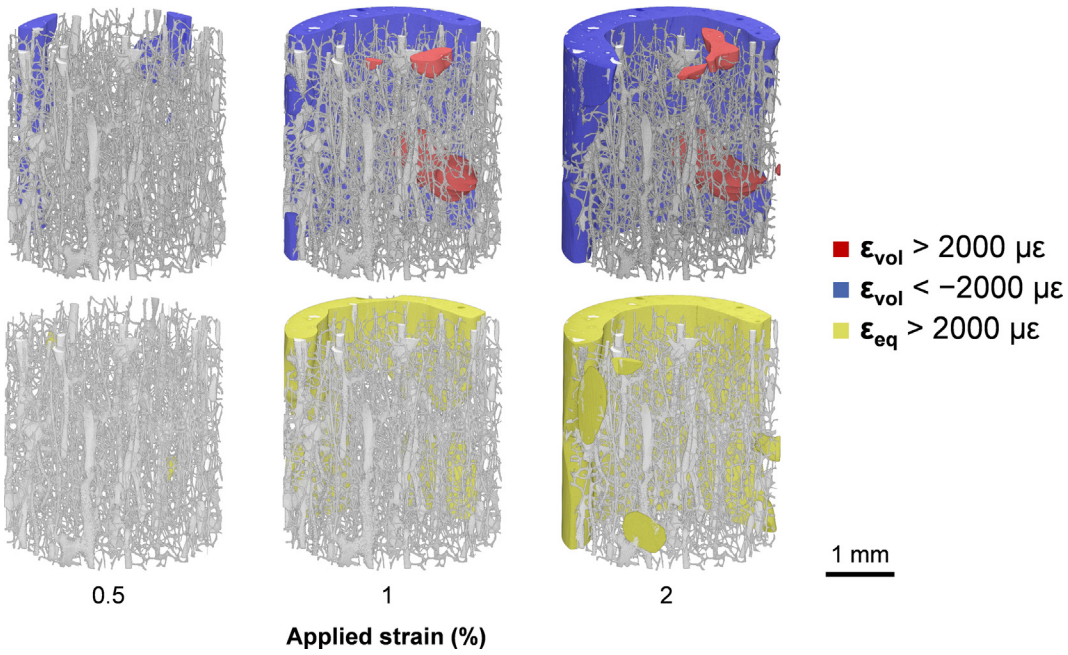

Fig. 3. 3D representation of highly strained regions in cortical bone specimen in Fig. 2 subjected to progressive compression test. (Top) High tensile (ε_{vol} > 2000 με) and compressive (ε_{vol} < −2000 με) strains are displayed for the specimen under each step of applied compression and (bottom) high residual strains (ε_{eq} > 2000 με) for the unloaded specimen.

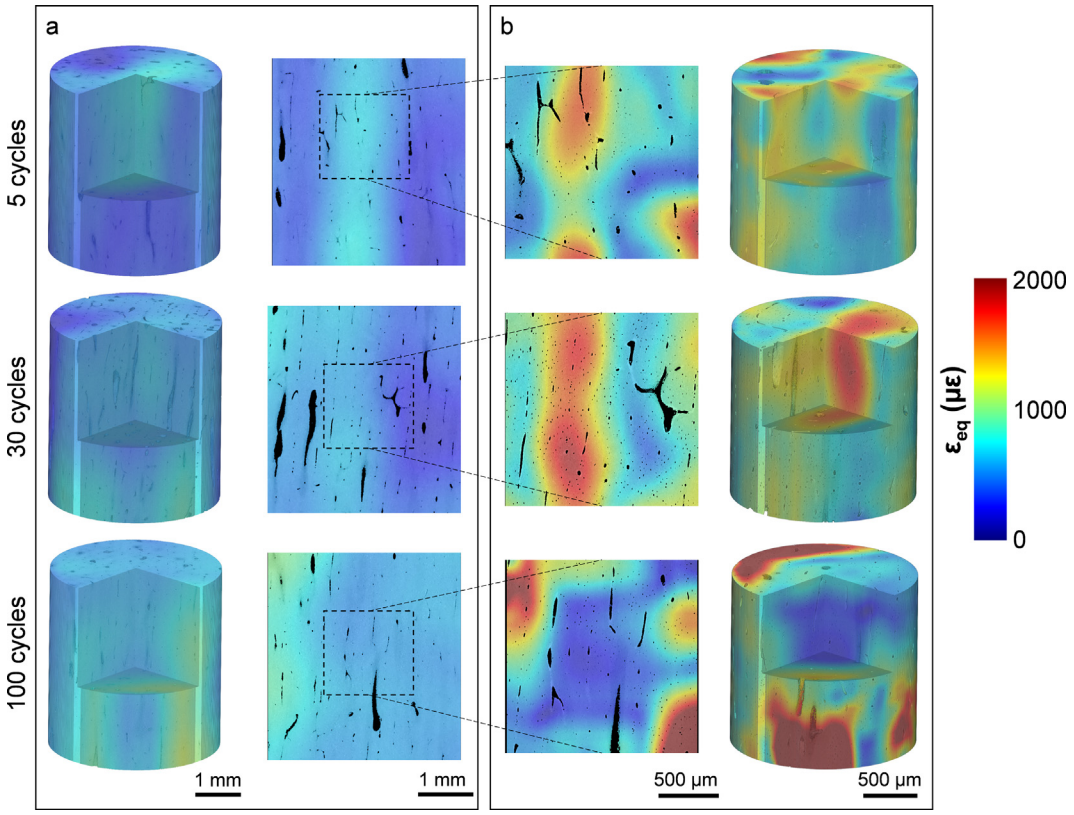

Fig. 4. 3D full-field von Mises equivalent strain distribution (ε_{eq}) after 5, 30 and 100 cycles of uniaxial compression computed using DVC on the (a) entire specimen diameter (5 μm voxel size images, with 320 μm DVC-spatial resolution) and (b) a volume of interest (VOI) in the centre of the specimen (2 μm voxel size images, with 96 μm DVC-spatial resolution). ε_{eq} distribution is shown for the entire volume and a representative longitudinal cross-section.

the presence of high local residual strains as an indicator of micro-damage could only be appreciated at the tissue level (Fig. 4b). The inhomogeneity of local strains in the bone matrix was previously described by Nicolella et al. (2005) and Hoc et al. (2006) at a higher resolution (up to 0.4 μm) using digital image correlation based on optical microscopy images. In agreement with those studies, local

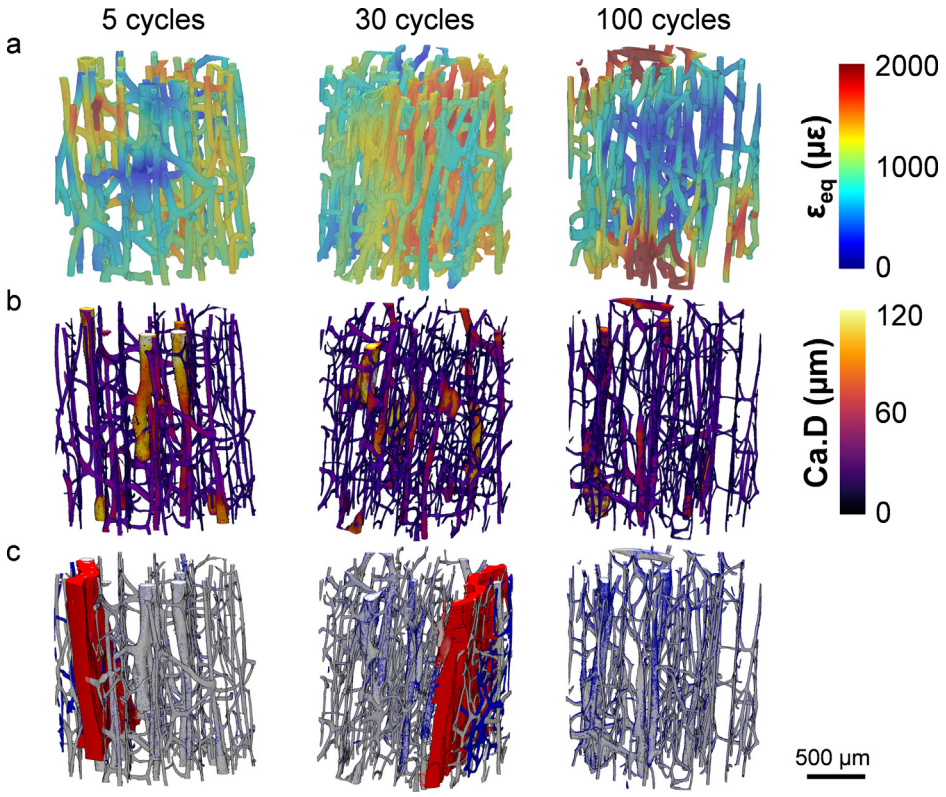

Fig. 5. Spatial correlation of local residual strains, cortical canal network morphometry and microdamage in cortical bone specimens subjected to 5, 30 and 100 cycles of uniaxial compression. (a) Local von Mises equivalent strain distribution (ε_{eq}) around the canal network (over 20 μm dilation of canals); (b) Colour map of canal network diameter (Ca.D) distribution; (c) Overlaid of the segmented canal network pre-failure (white), after failure (blue) and microcracks (red).

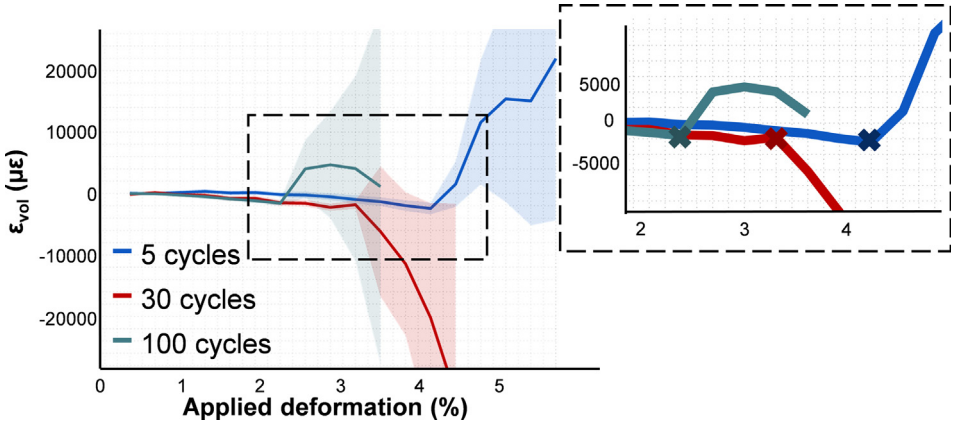

Fig. 6. DVC-computed volumetric strains (ε_{vol}) during continuous uniaxial compression after 5, 30 and 100 cycles. The solid lines represent the mean εvol values, with the shaded areas representing the standard deviation. The insert details the points (× symbols) prior to visible failure (i.e. microcracks).

residual tissue strains here were mostly above 2000 με, whereas microscopic average strains only accounted for 500 με. These results highlight the need for a multi-scale mechanical characterization of bone, as the macroscopic properties (i.e. modulus reduction, global residual strains) are not sufficient to accurately predict the source and potential incidence of damage due to local residual strains build-up in the tissue.

Cortical bone mechanical properties are strongly governed by its microstructure and intracortical porosity has previously been reported to explain a significant amount of variance in bone strength and fatigue life (Carter et al., 1976; Loundagin et al., 2020; Turnbull et al., 2014; Zioupos et al., 2008). Particular attention has also been given to the contribution of canal diameter as a predictor of the overall fatigue behavior of cortical bone (Loundagin et al., 2020; Yeni et al., 1997), with vascular canals as stress concentrators. In the current study, highest local residual strains (i.e. above 1500 με) following cyclic loading were observed in regions with thinnest canals (Fig. 5). Despite the presence of a high number of smaller canals in cortical bone may increase its fracture toughness and fatigue life (Loundagin et al., 2020; Yeni et al., 1997), the DVC-computed ε_{eq} suggested that localized areas with the thinnest canals may accumulate more microdamage due to larger amount of stress concentration in which microcracks typically initiate. Interestingly, such highly strained regions after 5 and 10 compressive cycles could predict the location where fracture occurred following overloading (Fig. 5). Conversely, fracture

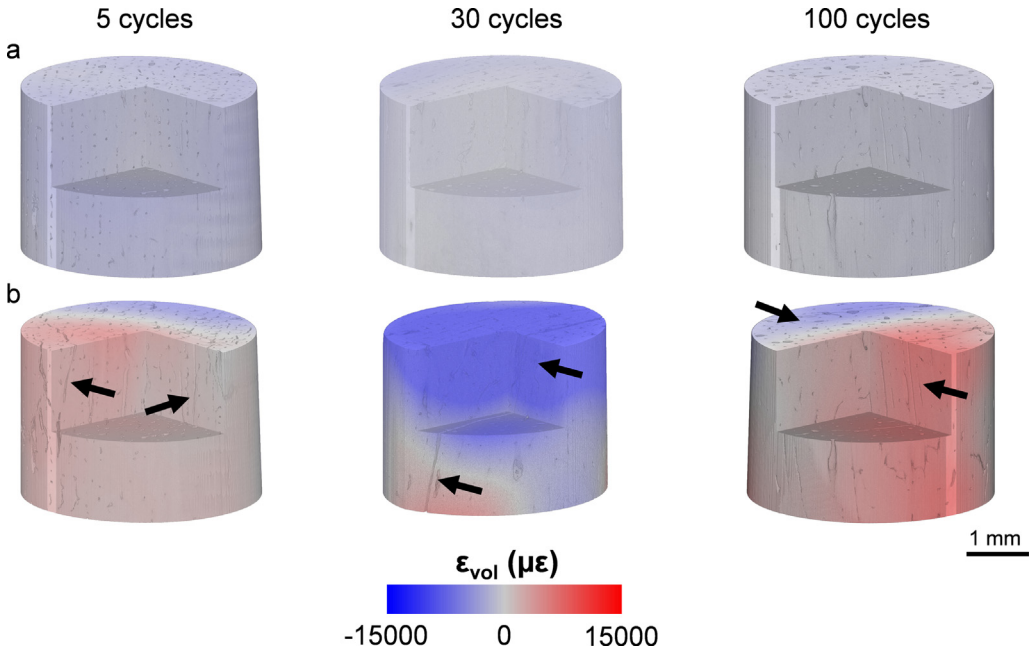

Fig. 7. 3D full-field volumetric strain distribution (ε_{vol}) (a) before and (b) after failure during continuous compression after 5, 30 and 100 cycles of uniaxial compression. Microcracks after failure are indicated with black arrows. The εvol evolution during continuous compression can be seen in the supplementary video.

in the more cycled specimen (i.e. 100 cycles) could not be identified within the imaged FOV despite an evident force drop was observed in the mechanical curve (Fig. S4), suggesting the main failure may have occurred outside the FOV. To better understand the effect that damage accumulation may have had on the overall fracture outcome, the final in situ SR-XCT test investigated the full-field ε_{vol} distribution during continuous compression, showing a major fracture throughout the specimens subjected to 5 and 10 cycles and several cracks progressively propagating through the most cycled specimen (100 cycles) (Supplementary Video 1). Following cyclic loading, some damage had already occurred and the ability of bone to progress further damage would decrease, leading to a decrease in fracture initiation toughness (Fletcher et al., 2014). This in line with the lower ε_{vol} magnitudes (i.e. below 3000 με in compression) that such specimen (100 cycles) accumulated during continuous compression prior to failure, which eventually led to fracture in a more brittle way due to the reduced bone plasticity when compared to the less cycled specimens. Additionally, following failure, DVC-computed strains based on real-time compression indicated tensile strain in regions where cracks opened and compressive strain in highly compacted areas (Fig. 7b, Supplementary video 1).

This study has some limitations. A small number of specimens were used, making the study unable to support statistical analysis; therefore, providing a more qualitative than quantitative evaluation as typically achieved in high-resolution XCT-based DVC studies. Additionally, all experiments presented were performed on different specimens, hence a correlation between the observations could not be determined. Finally, the accumulation of residual strains at increasing compressive cycles was not conducted, due to the long acquisition time needed for high-resolution imaging; extending the duration of the test could impact the mechanical properties of bone due to the effect of X-ray irradiation (Barth et al., 2010; Marta Peña Fernández et al., 2018). Nonetheless, the combination of in situ high-resolution XCT imaging and DVC employed in this study allowed for a deeper understanding on the mechanical behavior and failure mechanisms of cortical bone following cyclic loading, showing for the first time 3D full-field residual strain accumulation at low cycles as a potential predictor of tissue failure due to overloading. The results reported in this study have the potential to produce a significant impact in the understanding of fracture mechanism in pathological conditions (i.e. osteoporosis), by further investigating the complex interplay of local residual strain accumulation, increased porosity and fatigue microcracks initiation/propagation pattern.

CRediT authorship contribution statement

Marta Peña Fernández: Conceptualization, Methodology, Validation, Formal analysis, Investigation, Data curation, Writing - original draft, Writing - reviewing & editing, Visualization, Project administration, Funding acquisition. **Alexander P. Kao:** Investigation, Writing - reviewing & editing. **Frank Witte:** Resources, Writing - reviewing & editing, Funding acquisition. **Hari Arora:** Investigation, Writing - reviewing & editing, Funding acquisition. **Gianluca Tozzi:** Conceptualization, Resources, Writing - reviewing & editing, Supervision, Project administration, Funding acquisition.

Declaration of Competing Interest

The authors declare that they have no known competing financial interests or personal relationships that could have appeared to influence the work reported in this paper.

Acknowledgement

The authors would like to acknowledge Roxane Bonithon, Andrew Bodey and Kazimir Wanelik for support during the experimental session at the Diamond-Manchester Imaging Branchline I13-2 at Diamond Light Source (UK) under proposal MG-22575. The Zeiss Global Centre (University of Portsmouth) provided X-ray facilities and software for image analysis. Funding from Biotrics biomaterials AG (Germany) supporting this study are gratefully acknowledged.

Appendix A. Supplementary data

Supplementary data to this article can be found online at https://doi.org/10.1016/j.jbiomech.2020.110105.

Reference

Atwood, R.C., Bodey, A.J., Price, S.W.T., Basham, M., Drakopoulos, M., 2015. A high-throughput system for high-quality tomographic reconstruction of large datasets at Diamond Light Source. Philos. Trans. R. Soc. A Math. Phys. Eng. Sci. 373. https://doi.org/10.1098/rsta.2014.0398.

Bajaj, D., Geissler, J.R., Allen, M.R., Burr, D.B., Fritton, J.C., 2014. The resistance of cortical bone tissue to failure under cyclic loading is reduced with alendronate. Bone 64, 57–64. https://doi.org/10.1016/j.bone.2014.03.045.

Barth, H.D., Launey, M.E., MacDowell, A.A., Ager, J.W., Ritchie, R.O., 2010. On the effect of X-ray irradiation on the deformation and fracture behavior of human cortical bone. Bone 46, 1475–1485. https://doi.org/10.1016/j.bone.2010.02.025.

Burr, D.B., Forwood, M.R., Fyhrie, D.P., Martin, R.B., Schaffler, M.B., Turner, C.H., 1997. Bone microdamage and skeletal fragility in osteoporotic and stress fractures. J. Bone Miner. Res. 12, 6–15. https://doi.org/10.1359/jbmr.1997.12.1.6.

Cardoso, L., Fritton, S.P., Gailani, G., Benalla, M., Cowin, S.C., 2013. Advances in assessment of bone porosity, permeability and interstitial fluid flow. J. Biomech. 46, 253–265. https://doi.org/10.1016/j.jbiomech.2012.10.025.

Carter, D.R., Hayes, W.C., Schurman, D.J., 1976. Fatigue life of compact bone—II. Effects of microstructure and density. J. Biomech. 9, 211–218. https://doi.org/10.1016/0021-9290(76)90006-3.

Christen, D., Levchuk, A., Schori, S., Schneider, P., Boyd, S.K., Müller, R., 2012. Deformable image registration and 3D strain mapping for the quantitative assessment of cortical bone microdamage. J. Mech. Behav. Biomed. Mater. 8, 184–193. https://doi.org/10.1016/j.jmbbm.2011.12.009.

Dall'Ara, E., Peña-Fernández, M., Palanca, M., Giorgi, M., Cristofolini, L., Tozzi, G., 2017. Precision of digital volume correlation approaches for strain analysis in bone imaged with micro-computed tomography at different dimensional levels. Front. Mater. 4. https://doi.org/10.3389/fmats.2017.00031.

Diab, T., Condon, K.W., Burr, D.B., Vashishth, D., 2006. Age-related change in the damage morphology of human cortical bone and its role in bone fragility. Bone 38, 427–431. https://doi.org/10.1016/j.bone.2005.09.002.

Doube, M., Kłosowski, M.M., Arganda-Carreras, I., Cordelières, F.P., Dougherty, R.P., Jackson, J.S., Schmid, B., Hutchinson, J.R., Shefelbine, S.J., 2010. BoneJ: Free and extensible bone image analysis in ImageJ. Bone 47, 1076–1079. https://doi.org/10.1016/j.bone.2010.08.023.

Fleck, C., Eifler, D., 2007. Influence of the loading rate on the cyclic deformation behaviour and the damage accumulation of cortical bone specimens under three-point bending. Adv. Eng. Mater. 9, 1069–1076. https://doi.org/10.1002/adem.200700281.

Fletcher, L., Codrington, J., Parkinson, I., 2014. Effects of fatigue induced damage on the longitudinal fracture resistance of cortical bone. J. Mater. Sci. - Mater. Med. 25, 1661–1670. https://doi.org/10.1007/s10856-014-5213-5.

Gauthier, R., Langer, M., Follet, H., Olivier, C., Gouttenoire, P.-J., Helfen, L., Rongiéras, F., Mitton, D., Peyrin, F., 2019. Influence of loading condition and anatomical location on human cortical bone linear micro-cracks. J. Biomech. 85, 59–66. https://doi.org/10.1016/j.jbiomech.2019.01.008.

Hoc, T., Henry, L., Verdier, M., Aubry, D., Sedel, L., Meunier, A., 2006. Effect of microstructure on the mechanical properties of Haversian cortical bone. Bone 38, 466–474. https://doi.org/10.1016/j.bone.2005.09.017.

Kim, J.H., Niinomi, M., Akahori, T., Toda, H., 2007. Fatigue properties of bovine compact bones that have different microstructures. Int. J. Fatigue 29, 1039–1050. https://doi.org/10.1016/j.ijfatigue.2006.09.018.

Loundagin, L.L., Haider, I.T., Cooper, D.M.L., Edwards, W.B., 2020. Association between intracortical microarchitecture and the compressive fatigue life of human bone: a pilot study. Bone Reports 12. https://doi.org/10.1016/j.bonr.2020.100254.

Mirzaali, M.J., Bürki, A., Schwiedrzik, J., Zysset, P.K., Wolfram, U., 2015. Continuum damage interactions between tension and compression in osteonal bone. J. Mech. Behav. Biomed. Mater. 49, 355–369. https://doi.org/10.1016/j.jmbbm.2015.05.007.

Morgan, E.F., Lee, J.J., Keaveny, T.M., 2005. Sensitivity of multiple damage parameters to compressive overload in cortical bone. J. Biomech. Eng. 127. https://doi.org/10.1115/1.1933916.

Morgeneyer, T.F., Taillandier-Thomas, T., Helfen, L., Baumbach, T., Sinclair, I., Roux, S., Hild, F., 2014. In situ 3-D observation of early strain localization during failure of thin Al alloy (2198) sheet. Acta Mater. 69, 78–91. https://doi.org/10.1016/j.actamat.2014.01.033.

Nalla, R.K., Kruzic, J.J., Kinney, J.H., Ritchie, R.O., 2005. Aspects of in vitro fatigue in human cortical bone: time and cycle dependent crack growth. Biomaterials 26, 2183–2195. https://doi.org/10.1016/j.biomaterials.2004.05.024.

Nicolella, D., Bonewald, L., Moravits, D., Lankford, J., 2005. Measurement of microstructural strain in cortical bone. Eur. J. Morphol. 42, 23–29. https://doi.org/10.1080/09243860500095364.

Nyman, J.S., Leng, H., Neil Dong, X., Wang, X., 2009a. Differences in the mechanical behavior of cortical bone between compression and tension when subjected to progressive loading. J. Mech. Behav. Biomed. Mater. 2, 613–619. https://doi.org/10.1016/j.jmbbm.2008.11.008.

Nyman, J.S., Roy, A., Reyes, M.J., Wang, X., 2009b. Mechanical behavior of human cortical bone in cycles of advancing tensile strain for two age groups. J. Biomed. Mater. Res. 89, 521–529. https://doi.org/10.1002/jbm.a.31974.

O'Brien, F.J., Taylor, D., Clive Lee, T., 2007. Bone as a composite material: the role of osteons as barriers to crack growth in compact bone. Int. J. Fatigue 29, 1051–1056. https://doi.org/10.1016/j.ijfatigue.2006.09.017.

Palanca, M., Cristofolini, L., Dall'Ara, E., Curto, M., Innocente, F., Danesi, V., Tozzi, G., 2016. Digital volume correlation can be used to estimate local strains in natural and augmented vertebrae: an organ-level study. J. Biomech. 49, 3882–3890. https://doi.org/10.1016/j.jbiomech.2016.10.018.

Peña Fernández, M., Barber, A.H., Blunn, G.W., Tozzi, G., Fern, A.A., 2018a. Optimization of digital volume correlation computation in SR-microCT images of trabecular bone and bone-biomaterial systems. J. Microsc. 272, 213–228. https://doi.org/10.1111/jmi.12745.

Peña Fernández, M., Black, C., Dawson, J., Gibbs, D., Kanczler, J., Oreffo, R.O.C., Tozzi, G., 2020. Exploratory full-field strain analysis of regenerated bone tissue from osteoinductive biomaterials. Materials (Basel). 13, 168. https://doi.org/10.3390/ma13010168.

Peña Fernández, M., Cipiccia, S., Dall'Ara, E., Bodey, A.J., Parwani, R., Pani, M., Blunn, G.W., Barber, A.H., Tozzi, G., 2018b. Effect of SR-microCT radiation on the mechanical integrity of trabecular bone using in situ mechanical testing and digital volume correlation. J. Mech. Behav. Biomed. Mater. 88, 109–119. https://doi.org/10.1016/j.jmbbm.2018.08.012.

Peña Fernández, M., Dall'Ara, E., Bodey, A.J., Parwani, R., Barber, A.H., Blunn, G.W., Tozzi, G., 2019. Full-field strain analysis of bone–biomaterial systems produced by the implantation of osteoregenerative biomaterials in an ovine model. ACS Biomater. Sci. Eng. 5, 2543–2554. https://doi.org/10.1021/acsbiomaterials.8b01044.

Reilly, G.C., Currey, J.D., 1999. The development of microcracking and failure in bone depends on the loading mode to which it is adapted. J. Exp. Biol. 202, 543–552.

Schaffler, M.B., Choi, K., Milgrom, C., 1995. Aging and matrix microdamage accumulation in human compact bone. Bone 17, 521–525. https://doi.org/10.1016/8756-3282(95)00370-3.

Schindelin, J., Arganda-Carreras, I., Frise, E., Kaynig, V., Longair, M., Pietzsch, T., Preibisch, S., Rueden, C., Saalfeld, S., Schmid, B., Tinevez, J.-Y., White, D.J., Hartenstein, V., Eliceiri, K., Tomancak, P., Cardona, A., 2012. Fiji: an open-source platform for biological-image analysis. Nat. Methods 9, 676–682. https://doi.org/10.1038/nmeth.2019.

Tozzi, G., Zhang, Q.H., Tong, J., 2014. Microdamage assessment of bone-cement interfaces under monotonic and cyclic compression. J. Biomech. 47, 3466–3474. https://doi.org/10.1016/j.jbiomech.2014.09.012.

Turnbull, T.L., Baumann, A.P., Roeder, R.K., 2014. Fatigue microcracks that initiate fracture are located near elevated intracortical porosity but not elevated mineralization. J. Biomech. 47, 3135–3142. https://doi.org/10.1016/j.jbiomech.2014.06.022.

Voide, R., Schneider, P., Stauber, M., Wyss, P., Stampanoni, M., Sennhauser, U., van Lenthe, G.H., Müller, R., 2009. Time-lapsed assessment of microcrack initiation and propagation in murine cortical bone at submicrometer resolution. Bone 45, 164–173. https://doi.org/10.1016/j.bone.2009.04.248.

Wang, X., Nyman, J.S., 2007. A novel approach to assess post-yield energy dissipation of bone in tension. J. Biomech. 40, 674–677. https://doi.org/10.1016/j.jbiomech.2006.02.002.

Winwood, K., Zioupos, P., Currey, J.D., Cotton, J.R., Taylor, M., 2006a. Strain patterns during tensile, compressive, and shear fatigue of human cortical bone and implications for bone biomechanics. J. Biomed. Mater. Res. 79A, 289–297. https://doi.org/10.1002/jbm.a.30796.

Winwood, K.L., Zioupos, P., Currey, J.D., Cotton, J.R., Taylor, M., 2006b. The importance of the elastic and plastic components of strain in tensile and compressive fatigue of human cortical bone in relation to orthopaedic biomechanics. J. Musculoskelet. Neuronal Interact. 6, 134–141.

Wolfram, U., Schwiedrzik, J., 2016. Post-yield and failure properties of cortical bone. Bonekey Rep. 5, 1–10. https://doi.org/10.1038/bonekey.2016.60.

Yeni, Y.N., Brown, C.U., Wang, Z., Norman, T.L., 1997. The influence of bone morphology on fracture toughness of the human femur and tibia. Bone 21, 453–459. https://doi.org/10.1016/S8756-3282(97)00173-7.

Zioupos, P., Currey, J.D., 1998. Changes in the stiffness, strength, and toughness of human cortical bone with age. Bone 22, 57–66. https://doi.org/10.1016/S8756-3282(97)00228-7.

Zioupos, P., Currey, J.D., Casinos, A., 2001. Tensile fatigue in bone: are cycles-, or time to failure, or both, important?. J. Theor. Biol. 210, 389–399. https://doi.org/10.1006/jtbi.2001.2316.

Zioupos, P., Gresle, M., Winwood, K., 2008. Fatigue strength of human cortical bone: age, physical, and material heterogeneity effects. J. Biomed. Mater. Res. – Part A 86, 627–636. https://doi.org/10.1002/jbm.a.31576.

Zioupos, P., Wang, X.T., Currey, J.D., 1996. The accumulation of fatigue microdamage in human cortical bone of two different ages in vitro. Clin. Biomech. 11, 365–375. https://doi.org/10.1016/0268-0033(96)00010-1.